Available online at www.sciencedirect.com
SCIENCE DIRECT®

Journal of the European Ceramic Society 23 (2003) 2039–2046

www.elsevier.com/locate/jeurceramsoc

Mechanisms of energy absorption in the creep fracture of woven ceramic composites

L. Casas[a,b], J.M. Martínez-Esnaola[a,b,*]

[a]CEIT—Centro de Estudios e Investigaciones Técnicas de Gipuzkoa, P. Manuel Lardizabal 15, 20018 San Sebastián, Spain
[b]Escuela Superior de Ingenieros, TECNUN, Universidad de Navarra, P. Manuel Lardizabal 13, 20018 San Sebastián, Spain

Received 18 July 2002; received in revised form 11 December 2002; accepted 15 December 2002

Abstract

A micromechanical model is developed which accounts for the energy absorbed in the creep deformation and fracture of a 2.5D SiC/C/SiC composite, representative of the new generation of non-oxide CMCs. The model quantifies the influence of the geometrical, mechanical and material parameters and, in particular, is very sensitive to the interfacial sliding stress. The effect of the sliding stress on the contribution of the different energy absorbing mechanisms in the creep fracture of CMCs is described. It is concluded that, for all testing conditions, most of the energy absorbed in the creep fracture is controlled by fibre–matrix debonding and fibre pull-out.

Keywords: Composites; Creep; Fracture; Interfaces; Modelling; SiC/SiC

1. Introduction

During the eighties ceramic matrix composites (CMCs) have been the subject of study due to their promising properties for high temperature applications. Much work has been oriented to understand and describe the behaviour of different CMC systems under monotonic, bending, creep and fatigue conditions at different ranges of stress and temperature.[1–3] In particular, time-dependent crack propagation and creep behaviour of ceramic composites have been analysed in a number of works,[4–8] most of them dealing with the problem of a single dominant matrix crack, and therefore not applicable when matrix cracks have saturated in density in the composite.[5,7] An important concern for a better knowledge of the high temperature behaviour of these materials is the identification and quantification of the different mechanisms of damage and energy absorption. Well known micromechanisms, such as matrix cracking, fibre-matrix debonding, fibre pull-out and oxidation, have been found and reported as the most important damage mechanisms.[9] Following testing and fractographic analyses, appropriate models should be used to determine the parts and the properties of the material that need a specific improvement and to reduce the effect of these damage modes.

This work presents a micromechanical model of the energy absorption mechanisms in the creep deformation and fracture of a SiC/C/SiC composite representative of the modern generation of non-oxide CMC systems. The model emphasises the critical role of the interfacial sliding stress.

2. Material

The material used in this investigation, CERASEP® 410, is a silicon carbide based ceramic matrix composite produced using chemical vapour infiltration (CVI) by the Société Européene de Propulsion (initially SEP, a division of Snecma, France). The multilayered ceramic matrix contains distinct layers of SiC, B_4C and SiBC, and is reinforced with SiC Hi-Nicalon™ fibres (produced by Nippon Carbon Co., Japan). Before matrix infiltration, the preforms are coated with a carbon

* Corresponding author. Tel.: +34-943-212800; fax: +34-943-213076.
E-mail addresses: jmesnaola@ceit.es (J.M. Martínez-Esnaola), lcasas@ceit.es (L. Casas).

0955-2219/03/$ - see front matter © 2003 Elsevier Science Ltd. All rights reserved.
doi:10.1016/S0955-2219(03)00029-3

interface to decrease the interface bonding between the fibres and the matrix. The composite material is formed by fibre bundles in a 2.5D architecture. The diameter of the fibres is about 15 μm and each bundle consists of approximately 500 fibres. The multilayered SiC based matrix is described in the literature as being self healing.[10–12] This relies on initial cracking to allow limited oxygen ingress, and this in turn leads to the formation of a borosilicate glass that flows, plugging the cracks and preventing further oxygen ingress.

3. Experimental procedure and creep results

Creep tests were carried out in air at stresses between 115 and 300 MPa and temperatures of 1000, 1100 and 1300 °C. The tests were performed in a servohydraulic testing machine (MTS-819) under load control. The applied load was controlled with a loading cell of 25 kN and precision over 0.001%. The strain was measured with a water-cooled high temperature extensometer (MTS 632.59, class A, with error in strain measurement less than 10^{-5}) with SiC rods and a gauge length of 25 mm. A heating rate of 20 °C/min was applied in all tests using a radiation furnace (MTS 653.02, with temparature control of ±1 °C). Fig. 1 shows the results of the creep testing campaign. The temperature and stress of each test are also indicated in the insert of Fig. 1. Note that different loading steps were applied (by incrementing the loads) in some tests. This of course invalidates the times to failure measured in those tests. However, the method has the advantage that steady state creep rates can be determined at various stress levels at constant temperature in a single test, although the effects of stress redistributions prior to the load increments have not been accounted for.

After fracture, optical (Microscope Reichter MEF4A) and scanning electron microscopy, SEM, (Philips XL30-CP) were used for a detailed fractographic analysis and microstructural characterisation, including the measurement of volume fraction of constituents, fibre pull-out length, matrix crack spacing, etc. Details of these analyses have been reported by Casas et al.[11,13] Push-in tests were performed for the interfacial characterisation of the as-received and the creep tested material[14] using a nanoindentation system (NanoIndenter II, Nano Instruments, Inc., Oak Ridge, TN, USA). Then the model proposed by Hsueh[15] was used to extract a number of interfacial parameters from the push-in experiments.

4. Modelling of energy absorption

An energy balance is performed in this section in order to determine the contribution of the main damage mechanisms at the different creep conditions. The analysis of energy absorption follows the ideas proposed by Puente et al.[16] for monotonic loading, which are extended here for high temperature creep deformation and fracture. Four main mechanisms of energy absorption during the fracture process have been considered: (i) fracture of 0° bundles, (ii) fracture of 90° bundles, (iii) interface debonding, and (iv) fibre pull-out. In addition to the energy dissipated in these mechanisms, the energy absorbed in the irreversible (macroscopic) creep deformation itself has also been considered.

The analysis described in the following sections is referred to a unit cell consisting of a cylindrical volume of a longitudinal bundle of section A and length L, as shown in Fig. 2. Note that an important simplification of this approach is that the effects of the transverse bundles on the longitudinal ones and on the whole composite (architecture effect) are not accounted for.

For convenience, and to facilitate the comparisons, the energy balance is subsequently established per unit volume of longitudinal bundle.

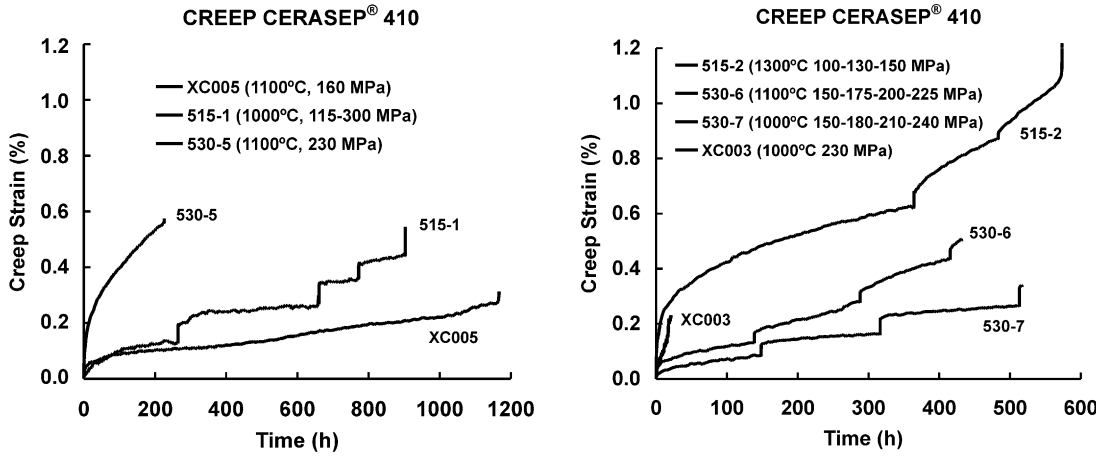

Fig. 1. Creep strain vs. time curves.

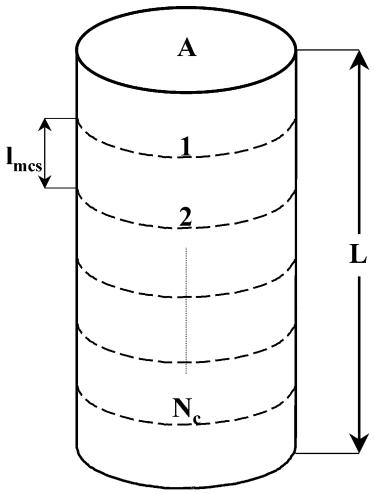

Fig. 2. A cylindrical volume of bundle containing N_c equally spaced cracks taken as reference for energy calculations.

4.1. Energy dissipated in fracture of 0° bundles

From Fig. 2, the cracked area of bundle, A_c, can be obtained as

$$A_c = AN_c \tag{1}$$

where A is the cross sectional area of the bundle and N_c is the number of cracks in the length L. The cracked area of matrix, A_{mc}, can be calculated using the volume fraction of matrix, V_m, as

$$A_{mc} = AN_cV_m \tag{2}$$

The work necessary to cause this matrix cracking, W_0, is then given by

$$W_0 = AN_cV_mG_m \tag{3}$$

where G_m is the fracture energy of the matrix. And finally, the energy absorbed in fracture of 0° bundles, U_0, per unit volume of bundle is given by

$$U_0 = \frac{W_0}{AL} = \frac{N_cV_mG_m}{L} = \frac{V_mG_m}{l_{mcs}} \tag{4}$$

where l_{mcs} is the matrix crack spacing.

4.2. Energy dissipated in fracture of 90° bundles

As observed in the fractographic analysis reported for this material,[13] cracks in the 90° bundles propagate along the interfaces, crossing the matrix between consecutive fibre-matrix interfaces, and without breaking fibres (Fig. 3). However, upper and lower bounds for the energy consumption in the fracture process can be obtained by considering the limit situations where either all the cracked area is matrix or all the cracked area is interface. Assuming that the volume fraction of bundles is the same in 0° and in 90° and using the cracked area of bundle obtained in (1), the necessary work to produce

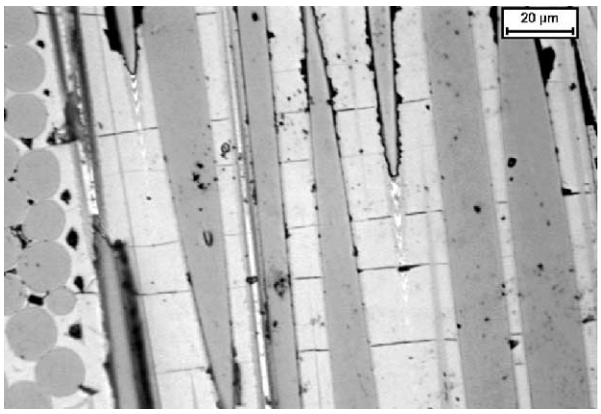

Fig. 3. Crack path without breaking fibres in loading direction (vertical).

matrix cracking of the 90° bundles, W_{90}, can be estimated using the average of the upper and lower bounds as

$$W_{90} = AN_c\frac{G_m + G_i}{2} \tag{5}$$

where G_m and G_i are the fracture energies of the matrix and the interface, respectively, and the term $(G_m + G_i)/2$ represents the average of fracture energies for the two bounds mentioned above. Then, the energy absorbed per unit volume of bundle, U_{90}, can be calculated as

$$U_{90} = \frac{W_{90}}{AL} = \frac{N_c(G_m + G_i)}{2L} = \frac{G_m + G_i}{2l_{mcs}} \tag{6}$$

where the same matrix crack spacing as in 0° bundles, l_{mcs}, is used. This is approximately true in average, as measured in the post-mortem analysis.[13]

4.3. Energy dissipated in interface debonding

After matrix cracking, stress transfer between matrix and fibres takes place due to interfacial shear. Along the transfer length, the stress in the matrix increases from zero at the matrix crack plane to the value corresponding to the compatibility of displacements between fibre and matrix. The stress in the fibre is then reduced from its maximum at the matrix crack plane to the value corresponding to the compatibility of displacements (Fig. 4).

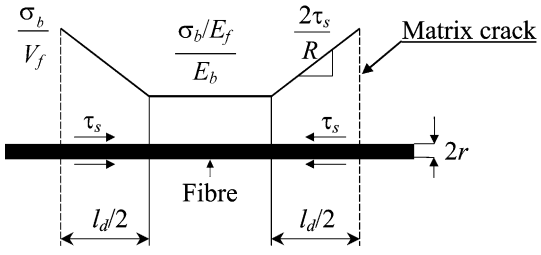

Fig. 4. Diagram showing load transfer between fibre and matrix. σ_b denotes the remote stress in the bundle.

The number of fibres that debond, N_{df}, can be estimated as

$$N_{df} = \frac{V_f A_c}{\pi r^2} \tag{7}$$

where V_f is the volume fraction of fibres, A_c is the cracked area of bundle given by (1), and r is the fibre radius. Then, the debonded area of fibres, A_d, is given by

$$A_d = 2\pi r l_d N_{df} \tag{8}$$

where $l_d/2$ is the debonded length on each side of the matrix crack plane (Fig. 4). The work necessary to produce the fibre-matrix debonding is then given by $W_d = A_d G_i$, and the energy absorbed per unit volume of bundle, U_d, can be calculated using (1), (7) and (8):

$$U_d = \frac{A_d G_i}{AL} = \frac{2V_f l_d G_i}{r l_{mcs}} \tag{9}$$

To determine the transfer length, $l_d/2$, a simple force equilibrium on the fibre gives (Fig. 4):

$$\frac{\sigma_b}{V_f} - \frac{2\tau_s}{r}\frac{l_d}{2} = \frac{\sigma_b E_f}{E_b} \tag{10}$$

and therefore

$$l_d = \frac{r\sigma_b V_m E_m}{\tau_s V_f E_b}$$

where σ_b is the axial stress in the bundle, $E_{f,m,b}$ are the Young's moduli of fibre, matrix and bundle, respectively, and τ_s is the interfacial sliding stress.

As the fibre debonds from the two free surfaces of each matrix crack, the maximum value for $l_d/2$ is given by one half the value of the crack spacing, $l_d = l_{mcs}$. Therefore, the actual value for $l_d/2$ will be the minimum between the value obtained from (10) and $l_d = l_{mcs}$.

4.4. Energy dissipated in fibre pull-out

The energy dissipated in fibre extraction can be estimated in terms of the mean pull-out length, l_f, and the interfacial sliding stress, τ_s (Fig. 5). A simple integration of the work done by the frictional forces upon extracting one single fibre, W_{1f}, gives:

$$W_{1f} = \int_0^{l_f} 2\pi r \tau_s x \mathrm{d}x = \pi r \tau_s l_f^2 \tag{11}$$

The number of broken fibres, N_{cf}, that will be extracted is:

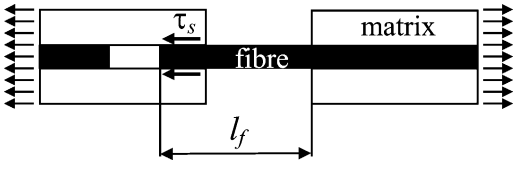

Fig. 5. Diagram of a single fibre extraction.

$$N_{cf} = \frac{AV_f}{\pi r^2} \tag{12}$$

The work necessary to extract the fibres can be calculated as $W_f = W_{1f} N_{cf}$, and therefore using (11) and (12) the energy absorbed per unit volume of bundle, U_f, is given by

$$U_f = \frac{W_{1f} N_{cf}}{AL} = \frac{\tau_s l_f^2 V_f}{rL} \tag{13}$$

4.5. Total dissipated energy

The total energy dissipated in the various damage mechanisms described above per unit volume of bundle, U_{TD}, can be estimated using Eqs. (4), (6), (9) and (13):

$$U_{TD} = U_0 + U_{90} + U_d + U_f \tag{14}$$

The energy dissipated at specimen level (i.e., per unit volume of composite), U_{TDS}, can be obtained multiplying the above energy by the volume fraction of longitudinal bundles, V_b, at the specimen:

$$U_{TDS} = U_{TD} V_b \tag{15}$$

In addition, the energy absorbed in the irreversible creep deformation (ε_c) itself, U_{CD}, must also be considered, so that the total energy absorbed in the test, U_{total}, is predicted as $U_{total} = U_{TDS} + U_{CD}$. The value of U_{CD} has been calculated assuming a steady state creep deformation for each test as

$$U_{CD} = \int_0^{t_f} \sigma \dot{\varepsilon}_c \mathrm{d}t = \sum_{i=1}^{N_{LS}} \sigma_i \Delta t_i A \sigma_i^n \exp\left(-\frac{Q}{RT}\right) = A\exp\left(-\frac{Q}{RT}\right)\sum_{i=1}^{N_{LS}} \sigma_i^{n+1} \Delta t_i \tag{16}$$

where t_f is the time to failure, N_{LS} is the number of loading steps in the test, σ_i and Δt_i are the stress and hold time, respectively, at the i-th loading step. R is the gas constant ($R = 8.314$ J/mol K), and A, n and Q are determined from fitting to steady state creep strain rates.[11] In particular, a stress exponent $n = 3.97$ has been found, which is not far from the range between 1.96 and 3.04 reported for Hi-Nicalon fibres at these temperatures.[17] This indicates that, in these tests, the creep behaviour of the composite in the steady state is controlled by the creep of the fibres. Note that this is the situation when matrix microcracking has occurred during loading, as in the present tests, and this in turn depends on the stress and temperature in the test.

5. Results and discussion

For the application of the analysis described in the previous sections, the fracture energies of matrix and

interface (G_m and G_i) and the interfacial sliding stress, τ_s, have to be computed. These are discussed in the following.

The model proposed by Marshall[18] has been used to calculate the interface fracture energy G_i. In addition to the elastic properties of fibre and matrix, the application of this model requires the debonding stress, σ_{db}, and the axial residual stresses, σ_{f0}, to be determined. The debonding stress has been obtained directly from push-down tests and the axial residual stresses have been calculated using the model proposed by Hsueh[15] for the interpretation of the push-down tests.[14] This is considered the most complete model for push-down tests, as it accounts for friction at the interface, Poisson's effects and residual stresses.[19] This model has also been applied to determine the interfacial sliding stress τ_s, as will be shown later on. Although the choice of τ_s is critical in the analysis, and in particular the evolution of the in situ interfacial shear during the test, in this work estimates of τ_s have been performed on post-mortem specimens. Nanoindentation push-down tests have been performed at room temperature in the as-received material and in samples tested at 1000, 1100 and 1300 °C.[14] The manufacturing temperature reported for a mini-composite of a similar material (Nicalon/C/SiC) is about 950 °C[20] so the thermal residual stresses at this temperature have been assumed to be null. As a first approach to obtain the value of residual stresses at the testing temperature, a simple linear interpolation between room temperature and the testing temperature has been used, assuming that the residual stresses of the as-received material vanish at 950 °C. The values obtained for G_i as well as other material parameters[11,13,14] are shown in Table 1.

The fracture energy of the matrix has been calculated as

$$G_m = \frac{K_{IC}^2}{E_m} \tag{17}$$

where K_{IC} is the fracture toughness and E_m is the Young's modulus of the matrix (a value of 400 GPa has been used). A fracture toughness of about 5.5 MPa$\sqrt{m}$ has been reported for the case of quite pure sintered SiC.[21] Although it is doubtful that this is also true for the multilayered matrix SiC/B_4C/SiBC, no other data have been found. Hence using this value in (17), a fracture energy of 76 J/m^2 has been estimated for the matrix.

Two different methods have been used for the calculation of the sliding stress τ_s. The first method is based on push-down tests and the application of Hsueh's model as indicated above. The sliding stress has been found to increase with the time spent by the composite at high temperature, in agreement with the behaviour observed in minicomposites of similar (SiC/C/SiC) materials.[22] This is believed to be a consequence of the modifications in the interface microstructure and the presence of oxides and glassy phases at the interface. For simplicity, a linear relationship between τ_s and the time to rupture has been assumed to estimate the sliding stress in the case of sample 515-2 (where τ_s has not been obtained directly from push-down tests) using the values obtained for samples tested at 1000 and 1100 °C. In the second method, the sliding stress has been calculated using the expression proposed by Kimber and Keer[23] based on the Aveston–Cooper–Kelly (ACK) model:[24]

$$\tau_s = 1.34\frac{V_m \sigma_{mu} r}{2V_f l_{mcs}} \tag{18}$$

where the new variable σ_{mu} is the ultimate tensile strength of the matrix. The resulting values of τ_s are also shown in Table 1. Note however that the matrix crack spacing in this equation is the one at the end of the loading step, because very few matrix cracks are generated during creep at constant load. Therefore Eq. (18) does not exactly reflect the sliding stress after creep exposure.

As shown in Fig. 1, and mentioned earlier, creep tests have been performed under different steps of loading in order to evaluate the secondary steady state under different stress levels at the same temperature in a single test. The experimentally measured energy per unit volume of composite, U_{test}, absorbed in each test has been determined as

$$U_{test} = \int_0^{t_f} \sigma\dot{\varepsilon}\,dt = \sum_{i=1}^{N_{LS}} \left(\int_0^{t_{li}} \sigma\dot{\varepsilon}\,dt + \sigma_i \Delta\varepsilon_{ci} \right) \tag{19}$$

Table 1
Properties of matrix, fibres and interface

Sample	E_m (GPa)	E_f (GPa)	r (μm)	V_m	V_f	σ_{db} (MPa)	σ_{f0} (MPa)	G_i (J/m^2)	l_{mcs} (μm)	l_f (μm)	τ_s Hsueh (MPa)	τ_s ACK (MPa)
515-1	400	270	7.5	0.45	0.47	−2235	−37.9	19.2	383	240	67.4	8.94
515-2	400	270	7.5	0.34	0.54	−2089	4.6	12.0	109	367	45.2	10.48
530-5	400	270	7.5	0.39	0.50	−2352	−23.8	18.6	172	233	21.9	12.87
530-6	400	270	7.5	0.40	0.46	−2704	−23.8	25.1	223	222	36.1	10.56
530-7	400	270	7.5	0.39	0.49	−2744	−37.9	25.4	313	137	34.8	7.38
XC003	400	270	7.5	0.44	0.45	−1974	−37.9	17.6	157	181	34.4	21.25
XC005	400	270	7.5	0.56	0.34	−2159	−23.8	26.5	220	164	44.0	14.23

where σ_i is the stress at the i-th loading step, t_{li} is the loading time to increase the stress from σ_{i-1} to σ_i, and $\Delta\varepsilon_{ci}$ is the creep strain increment during the i-th hold time.

Tables 2 and 3 and Fig. 6 show the comparison between the experimental energy absorbed in each test and the predictions of the mechanistic model based on the two methods used to compute τ_s. It is important to notice that an unknown part of the external work turns into kinetic energy during the final fracture, and that this term should be added to the energy absorbed in the mechanisms described above. Although this kinetic energy has not been accounted for, the comparison is deemed to be satisfactory for the two estimates of the sliding stress, particularly if one bears in mind the scatter of the measured properties at the micro-level and that average values have been used in the predictions. However, important differences appear between the analyses based on the two estimates of τ_s if one considers the contribution of the individual mechanisms to the total damage (Table 4). When the sliding stress given by Hsueh's model is used, fibre pull-out and fibre-matrix debonding appear to be the main mechanisms, while the calculations based on the sliding stress obtained with the ACK model predict that fibre–matrix debonding is clearly the main damage mechanism. This aspect highlights once more the critical effect of the interfacial sliding stress. It is important to note that the

Table 2
Energy balance using the sliding stress obtained with Hsueh's model (MJ/m^3)

Sample	U_0	U_{90}	U_d	U_f	U_{TD}	V_b	U_{TDS}	U_{CD}	U_{total}	U_{test}	U_{total}/U_{test}
515-1	0.104	0.124	0.480	0.870	1.578	0.412	0.650	0.250	0.900	1.074	0.84
515-2	0.319	0.402	0.598	0.052	1.371	0.360	0.494	1.010	1.504	1.379	1.09
530-5	0.221	0.274	2.161	0.054	2.710	0.391	1.059	0.750	1.809	1.633	1.11
530-6	0.182	0.226	1.370	0.001	1.779	0.421	0.748	0.420	1.168	0.989	1.18
530-7	0.124	0.161	1.045	0.427	1.757	0.425	0.747	0.120	0.867	0.712	1.22
XC003	0.265	0.297	1.954	0.012	2.528	0.420	1.062	0.036	1.098	1.151	0.95
XC005	0.225	0.225	1.041	0.063	1.554	0.390	0.606	0.372	0.978	0.453	2.16

Table 3
Energy balance using the sliding stress obtained with ACK model (MJ/m^3)

Sample	U_0	U_{90}	U_d	U_f	U_{TD}	V_b	U_{TDS}	U_{CD}	U_{total}	U_{test}	U_{total}/U_{test}
515-1	0.104	0.124	2.425	0.116	2.769	0.412	1.140	0.250	1.390	1.074	1.29
515-2	0.319	0.402	1.729	0.012	2.462	0.360	0.886	1.010	1.896	1.379	1.37
530-5	0.221	0.274	2.464	0.032	2.991	0.391	1.168	0.750	1.918	1.633	1.17
530-6	0.182	0.226	3.106	0.001	3.515	0.421	1.478	0.420	1.898	0.989	1.92
530-7	0.124	0.161	3.302	0.091	3.678	0.425	1.563	0.120	1.683	0.712	2.36
XC003	0.265	0.297	2.117	0.007	2.686	0.420	1.128	0.036	1.164	1.151	1.01
XC005	0.225	0.225	2.157	0.020	2.627	0.390	1.025	0.372	1.397	0.453	3.09

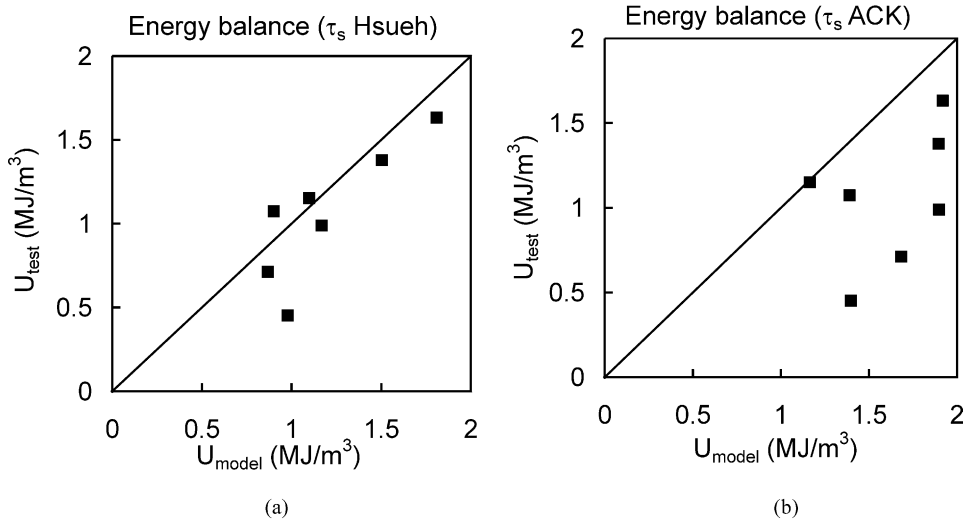

Fig. 6. Energy predicted by the model vs. energy absorbed in the test: (a) τ_s based on Hsueh's model; (b) τ_s based on ACK.

Table 4
Contribution of each damage mechanism (%) to the total damage of the specimen using τ_s obtained with Hsueh's model and with the ACK model

Sample	Hsueh				ACK			
	U_0	U_{90}	U_d	U_f	U_0	U_{90}	U_d	U_f
515-1	6.8	8.2	30	55	3.7	4.3	88	4.0
515-2	23	29	44	4.0	13	16	70	1.0
530-5	8.0	10	80	2.0	7.5	9.3	82	1.2
530-6	10	13	77	0.0	5.2	6.4	88	0.4
530-7	7.4	9.6	59	24	3.3	4.3	90	2.4
XC003	10	12	77	1.0	9.8	11	79	0.2
XC005	14	14	67	5.0	8.6	8.6	82	0.8

push-down tests have been performed at room temperature and that during creep testing the sliding stress is expected to be lower due to the existence of glassy phases that reduce the friction at the fibre–matrix interface. This aspect might explain that the energy predicted by the model is higher than that actually absorbed in the test. Nevertheless, the values of the sliding stress resulting from push-down tests appear to be more realistic than those given by the ACK prediction. The sliding stress has been observed to increase with the time of exposure at high temperature.[22] This is also the trend found in the τ_s values calculated in this work, as indicated earlier; however, the values given by the ACK model (based on the matrix crack spacing, that does not vary significantly during creep) do not follow this tendency. These observations underline the need for techniques to measure the in situ values of the interfacial sliding stress during the tests at high temperature, in combination with models and analyses that take into account the influence of the transverse bundles (architecture effect).

6. Conclusions

A micromechanical model of energy absorption in the high temperature creep deformation and fracture of a SiC/C/SiC composite has been presented. The model quantifies the influence of the mechanical and material parameters and, in particular, is very sensitive to the interfacial sliding stress. The effect of the sliding stress on the contribution of the different energy absorbing mechanisms in the creep fracture of CMCs has been assessed. It is concluded that fibre–matrix debonding and fibre pull-out are the most important damage mechanisms. Actually, the energy absorbed in the different fracture mechanisms has its origin in the elastic energy, which is released during the fracture process. The model may be refined by partitioning the total absorbed energy during the deformation and fracture processes into its elastic and inelastic components, for example via the evolution of the Young's modulus, which is widely recognised to be a good macroscopic measure of damage during deformation.

Acknowledgements

This work is part of the Brite-EuRam project BE97-4020 with financial support from the European Commission, co-ordinated by Rolls-Royce plc, in collaboration with Rolls-Royce Deutschland, MTU, ITP, Ansaldo Ricerche, Qinetiq (former DERA), IE (former IAM)-JRC Petten and CEIT. The authors also want to acknowledge the valuable comments received during the reviewing process.

References

1. Boitier, G., Vicens, J. and Chermant, J. L, Understanding the creep behavior of a 2.5D C_f–SiC composite. II. Experimental specifications and macroscopic mechanical creep responses. *Mat. Sci. Engng A*, 2001, **289**, 265–275.
2. Zhu, S., Mizuno, M., Nagano, Y., Cao, J., Kagawa, Y. and Kaya, H., Creep and fatigue behavior in an enhanced SiC/SiC composite at high temperature. *J. Am. Cer. Soc.*, 1998, **81**, 2269–2277.
3. Puente, I., Efecto de la Temperatura y Velocidad de Deformación en el Comportamiento Mecánico a Tracción de un Composite de Matriz Cerámica CAS/SiC, Tesis Doctoral, Escuela Superior de Ingenieros, Universidad de Navarra, San Sebastián, 1997.
4. Henager, C. H. Jr. and Jones, R. H., High-temperature plasticity effects in bridged cracks and subcritical crack growth in ceramic composites. *Mat. Sci. Engng*, 1993, **A166**, 211–220.
5. Begley, M. R., Evans, A. G. and McMeeking, R. M., Creep rupture in ceramic matrix composites with creeping fibers. *J. Mech. Physics Solids*, 1995, **43**, 727–740.
6. Iyengar, N. and Curtin, W. A., Time-dependent failure in fiber-reinforced composites by matrix and interface shear creep. *Acta Mater.*, 1997, **45**, 3419–3429.
7. Cox, B. N., Sridhar, N. and Argento, C. R., A bridging law for creeping fibres. *Acta Mater.*, 2000, **48**, 4137–4150.
8. Henager, C. H. jr and Hoagland, R. G., Subcritical crack growth in CVI SiC_f/SiC composites at elevated temperatures: dynamic crack growth model. *Acta Mater.*, 2001, **49**, 3739–3753.
9. Darzens, S., Chermant, J. L. and Vicens, J., Microcracking mechanism in a SiC_f–SiBC composite creep-tested in argon. *J Microscopy*, 2001, **201**, 230–237.
10. Darzens, S., Chermant, J. L. and Vicens, J., Microstructure and morphology of SiC_f/SiBC composites. *J. Eur. Phys. AP*, 2001, **15**, 35–48.
11. Casas, L., Elizalde, M. R., Martínez-Esnaola, J. M., Martín-Meizoso, A., Gil Sevillano, J., Claxton, E. and Doleman, P., Behavior of a 2.5D woven composite material SiC/SiC. In *High Temperature Ceramic Matrix Composites, HT-CMC4*, ed. W. Krenkel, R. Naslain and H. Schneider. Wiley-VCH, Weinheim, 2001, pp. 486–491.
12. Bouillon, E., Abbé, F., Goujard, S., Pestourie, E. and Habarou, G., Mechanical and thermal properties of a self-sealing matrix composite and determination of the life time duration. In 24th Annual Conference on Composites, Advanced Ceramics, Materials and Structures, Cocoa Beach, FL, USA, 2000. *Cer. Engng. Sci. Proc.*, 2000, **21**, 459–467.

13. Casas, L., Elizalde, M. R., Puente, I., Martínez-Esnaola, J. M., Martín-Meizoso, A. and Fuentes, M., Comportamiento a fluencia de un material compuesto tejido SiC/SiC. *Anales de Mecánica de la Fractura*, 2001, **18**, 316–320.
14. Casas, L., Elizalde, M. R. and Martínez-Esnaola, J. M., Interface characterisation and correlation with the creep behaviour of a 2.5D SiC/C/SiC composite. *Composites Part A*, 2002, **33**, 1449–1452.
15. Hsueh, C. H., Evaluation of interfacial properties of fiber-reinforced ceramic composites using a mechanical properties microprobe. *J. Am. Cer. Soc.*, 1993, **76**, 3041–3050.
16. Puente, I., Martín-Meizoso, A., Elizalde, M. R., Sánchez, J. M., Martínez-Esnaola, J. M. and Fuentes, M., Energy absorption in calcium aluminosilicate/SiC glass ceramic matrix composite tensile tests. *Mat. Sci. Tech.*, 1998, **14**, 974–979.
17. Bodet, R., Bourrat, X., Lamon, J. and Naslain, R., Tensile creep behaviour of a silicon carbide-based fibre with low oxygen content. *J. Mat. Sci.*, 1995, **30**, 661–677.
18. Marshall, D. B., Analysis of fiber debonding and sliding experiments in brittle matrix composites. *Acta Metall. Mat.*, 1992, **40**, 427–441.
19. Elizalde, M. R., Efecto de la Intercara en Materiales Compuestos de Matriz Cerámica y Fibras Continuas, Tesis Doctoral, Escuela Superior de Ingenieros, Universidad de Navarra, San Sebastián, 1997.
20. Bikok, M., Pailler, R. and Lamon, J., Prediction of the lifetime of mini-composites under static fatigue at high temperature-task I: manufacturing of test-specimens, LCTS Interim Report 1, 1998.
21. Kingery, W. D., Browen, H. K. and Uhlmann, D. R., *Introduction to Ceramics*. John Wiley & Sons, New York, 1976.
22. Rugg, K. L., Tressler, R. E. and Lamon, J., Interfacial behavior of microcomposites during creep at elevated temperatures. *J. Eur. Cer. Soc.*, 1999, **19**, 2297–2303.
23. Kimber, A. C. and Keer, J. G., On the theoretical average crack spacing in brittle matrix composites containing continuous aligned fibres. *J. Mat. Sci. Letters*, 1982, **1**, 353–354.
24. Aveston, J., Cooper, G. A. and Kelly, A., The properties of fibre composites, In *Proc. Conference on the Properties of Fibre Composites, National Physical Laboratory, Teddington, UK, Paper 2*. IPC Science and Technology Press Ltd., Guildford, 1971, pp. 15–26.